SPi	Journal Code				Article ID				Dispatch: 09.09.16	CE: Mary Charlane Payuan
	S	I	A		6	1	4	4	No. of Pages: 10	ME:

Research article

SURFACE and INTERFACE ANALYSIS

Received: 17 May 2016 Revised: 26 July 2016 Accepted: 28 August 2016 Published online in Wiley Online Library

(wileyonlinelibrary.com) DOI 10.1002/sia.6144

Energetic mixing of anti-SNAP25 on lipid monolayers: degree of saturation of C18 fatty acids

Q1 Lai Ti Gew[a,b] and Misni Misran[b]*

In our study, various mixtures of C18 fatty acids with different degrees of saturation in their hydrocarbon chain, namely stearic acid (SA), oleic acid (L1), linoleic acid (L2), and linolenic acid (L3), and a polyclonal antibody, anti-synaptosome-associated protein of 25 kDa (SNAP25) (AS25), have been investigated using the Langmuir–Blodgett (LB) technique accompanied by atomic force microscopy (AFM) imaging. The *cis*-double bonds in unsaturated lipids (L1, L2, and L3) have kinks in their molecular conformation and thus could not pack as tightly and uniformly as SA. The bends and kinks in the molecular structure may interfere with the packing of the lipid monolayer which will promote fluidity as shown in the analyzed compressibility modulus (C_s^{-1}) data. The negative values of Gibbs free energy of mixing (ΔG_{mix}) () of C18 fatty acids/AS25 confirm the spontaneity interaction of AS25 molecules on the monolayers. The amount of AS25 incorporated into the monolayer strongly affected the thermodynamic properties of the lipid monolayers. AFM surface roughness analyses also indicate that AS25 molecules are strongly bounded on the surface membrane as predicted by the obtained energetic data. In comparison to all C18 fatty acids studied, the strongest intermolecular interaction is observed in L1 at the investigated ranges. In particular, at mole ratio of 26:1, the most negative ΔG_{mix} is observed at L1. Thus, we can draw the conclusion that AS25 is best mixed with L1. This L1/AS25 ratio mimicking a half bilayer membrane serves as a very useful reference in preparing fatty-acid nanoimmunoliposomes as the targeted drug-delivery vehicles for cancer therapy. Copyright © 2016 John Wiley & Sons, Ltd.

Keywords: lipid–protein interactions; Langmuir–Blodgett technique; atomic force microscopy; intermolecular interactions; lipid bilayer; surface roughness

Introduction

Intermolecular interactions between antibodies and fatty acids play a critical role in developing new antibody-targeted liposome formulations and also serve as a reference to improve existing formulations that remain under studied. Antibody-targeted liposomes are made by conjugating antibodies to the lipid bilayer of a liposome surface which promotes a specific interaction with the cancer cells.[1–4] Pharmacokinetic analysis and therapeutic studies revealed that antibody-targeted liposomes have considerable potential to be used as a drug-delivery system (DDS) for cancer therapy. It optimizes the delivery of the drug to the tumor cells efficiently, reduces the exposure of highly toxic anticancer drug to healthy cells, and minimizes side effects.[5–8] A number of methods have been reported for coupling or conjugating antibodies or their fragments to the surface of liposomes. Manjappa *et al.* (2011) extensively reviewed several chemical strategies for the preparation of immunoliposomes;[9] however, very little work has been done on the antibody–fatty acid interactions using the Langmuir approach. Langmuir–Blodgett (LB) is an ideal tool for studying the thermodynamic behavior of lipid–protein mixed systems.[10–13] Parameters such as mean molecular area, compressibility modulus, and Gibbs free energy of mixing can be obtained from π–*A* isotherms in order to determine the miscibility and stability of the mixed system. Thermodynamic analysis will provide useful information on how antibodies associate to the membranes, their ability to form antibody-targeted liposomes, and a precise composition of fatty acids and antibodies required for forming antibody-targeted liposomes. LB technique is also one of the promising methods in the preparation of thin film with a thickness of one molecule as it enables deposition of the monolayer (or multilayers) over large area homogenously. Deposition of floating monolayers will be performed using LB to transfer the mixed monolayer of C18 fatty acids/AS25 onto a solid substrate, and then observed by tapping-mode atomic force microscopy (TM-AFM). AFM has been extensively used in biological imaging, because of its distinctive ability to provide valuable structural information at a single molecule level.[14–16] AFM can be operated with contact or non-contact mode (or also known as tapping mode). TM-AFM scanning is preferred for imaging weakly immobilized of membrane proteins structure, as the cantilever oscillates rapidly above the sample without damaging the delicate biological specimens. In comparison to the contact mode, tapping mode minimizes contact time, friction, and produce less lateral force, making it ideal for study the morphology of soft biomaterial.[17,18]

* *Correspondence to: Misni Misran, Department of Chemistry, Faculty of Science, University of Malaya, 50603 Kuala Lumpur, Malaysia. E-mail: misni@um.edu.my*

a *Department of Biological Sciences, Faculty of Science and Technology, Sunway University, No. 5, Jalan Universiti, Bandar Sunway, 47500, Petaling Jaya, Selangor, Malaysia*

b *Department of Chemistry, Faculty of Science, University of Malaya, Kuala Lumpur 50603, Malaysia*

Membrane protein functions are essentially influenced by membrane fluidity.[19–21] The binding of proteins to the membrane depends on membrane fluidity. Peripheral proteins are attached to the membrane surface by electrostatic interactions with lipid polar headgroups. Integral proteins interact directly with the hydrophobic hydrocarbon chain of the lipid bilayer. The cohesive attraction of integral proteins on the membrane is influenced by the degree of unsaturation of the hydrocarbon chain. In general, membrane fluidity is affected by the length and degree of unsaturation in the fatty acid chains. The most common fatty acids contain 12 to 22 carbon atoms. In this experiment, we have chosen saturated and unsaturated fatty acids with 18 carbon atoms, namely stearic acid (SA) (18:0), oleic acid (L1) (18:1), linoleic acid (L2) (18:2), and linolenic acid (L3) (18:3) to study their intermolecular interactions with a polyclonal antibody. The *cis*-double bonds in L1, L2, and L3 have a kink in their molecular conformation and could therefore not pack as tightly and uniformly as SA.[22–25] They are thermodynamically unstable compared to *trans* configuration. The bends and kinks in the molecular structure may interfere with the packing of the lipid monolayer which will promote fluidity. C18 fatty acids are used in this case in order to provide the monolayer its natural membrane environment using Langmuir monolayer techniques. Various volumes of a polyclonal antibody, namely anti-synaptosome-associated protein of 25 kDa (SNAP25) (AS25), were incorporated onto the monolayer.

AS25 is a polyclonal antibody produced in rabbits. Polyclonal antibodies are extensively used for research purposes. They are relatively inexpensive, and large quantities can be produced compared to monoclonal antibodies. It is useful when the nature of the antigen is unknown, and they are nonspecific which enables them to recognize multiple epitopes on antigens. The SNAP-25 antibody shows expression in the neuroblastoma cell line SH-SY5Y;[26] this cell line is widely used as an *in vitro* study model for Parkinson's disease.[27–29] In our future studies, we will use the findings from this work to further investigate incorporation of such protein into liposomes for specific targeting and the delivery of encapsulated drugs.

SNAP-25 is a soluble protein with a molecular weight of 25 kDa, containing 206 amino acids.[30] It is a membrane bound, presynaptic nerve terminal protein, which plays an essential role in vesicle membrane fusion events with the plasma membrane. In regulating neuronal exocytosis, SNAP-25 is a soluble *N*-ethylmaleimide-sensitive factor protein receptor (SNARE) protein complexes that is intrinsically water soluble, but anchored to presynaptic plasma membrane via four cysteine-linked likely fatty acylation site, and behaves as an integral protein.[31] In developing a DDS, it is also important to consider how to enhance the systems to be merged to the cancer (or tumor) cells in order for entrance the encapsulated drug into the cancer or tumor cell successfully. Membrane fusion plays a significant role in DDS in delivering the drug in the body.[32–35] Many fusion processes are mediated and regulated by SNARE proteins, such as, SNAP-25. It is one of the SNARE proteins that have been widely studied because they induce the extremely fast release of synaptic vesicles.[30,31,34,36,37] Our prediction is that the event of AS25 partially embedded onto the bilayer (and subsequently liposomes) will promote fusion of liposomes on the targeted site, where protein–protein interactions between SNAP-25 and AS25 will be taken place first on the cell membrane, which will then draw two lipid bilayers together, driving hemifusion and finally full fusion for the entry of the drugs.[34,36–38]

Our aims of this work are to compare the behavior of antibodies in saturated and unsaturated C18 fatty-acid monolayers and their behavior in different degree of unsaturation. We also hope to provide valuable information on the required composition of fatty acid and antibodies in preparing liposomal targeted drug delivery systems or proteoliposomes, or in membrane fusion explorations. The development of antibodies is complex and time consuming, leading to its high cost and relatively scarce availability.

Experimental section

Materials

C18 fatty acids such as SA, L1, L2, and L3, and the antibody AS25 (Product number S9684) were purchased from Sigma-Aldrich. AS25 is supplied as an IgG fraction of antiserum (developed in rabbit) in 0.1 M saline phosphate-buffered, pH 7.4, containing 15 mM sodium azide as a preservative and it is stored in −20 °C freezer. HPLC-grade methanol was purchased from Merck. Double-distilled water processed by using the NANOpure Diamond Ultrapure Water System was used as subphase throughout. Resistivity of water is 18.2 MΩ cm.

Measurement of Langmuir–Blodgett monolayers and mixed monolayers

Separate stock solutions of fatty acids were prepared in analytical-grade chloroform which was purchased from Merck. Spreading solutions were deposited randomly onto the water subphase (26 °C ± 0.1 °C) with Hamilton microsyringe precise to 0.5 μl. After spreading, the monolayers were left to equilibrate for about 5 min, and then an increasing volume of antibody solution (10 μl, 25 μl, 50 μl, 75 μl, and 100 μl, respectively) was added onto each monolayer formed. The desired volume of antibody solution was withdrawn from the vial directly without any dilution. We converted the amount of antibody solution used into mass by using the concentration stated in the given product sheet, which is 9.55 μg/μl. This mole ratio of fatty acids to antibody was used in all the plotted graphs and data analysis in this paper.

Surface pressure (π)–molecular area (A) isotherms were obtained by using a computer-controlled KSV 5000 (Finland) Langmuir balance furnished with symmetric barriers and Teflon trough of total area of 48 840 mm^2 (407 mm × 120 mm) and equipped with a roughness surface platinum Wilhelmy plate (19.62 mm × 10.00 mm); its total length is 39.80 mm. Monolayers were compressed at a rate of 10 mm min^{-1}.

Determination of K_{ow} by RP-HPLC

Twenty microliters of AS25 was added into two separate vials: (i) 1 ml of nanopure water; and (ii) mixture of 1:1 octanol–water. A series of dilution of aqueous solution of AS25 were also prepared to enable us to plot a standard curve. Solutions were homogeneously mixed using shaker powered by electric motor at speed of 250 rpm for 10 min. The solutions were then left to stand for 30 min to achieve equilibrium prior to HPLC analysis.

HPLC analysis of AS25 was carried out using a Shimadzu reverse phase-high performance liquid chromatography (RP-HPLC) system with Merck Chromolith® ODS C18 HPLC column (length: 100 mm × 4.6 mm I.D., pore size: 2 μm) equipped with photodiode array detector (PDA) and auto-injector. Detection of AS25 using PDA was observed at 200 to 500 nm as the reference wavelength. The mobile phase was methanol–water (50/50, v/v). All peak areas were obtained by averaging the results of at least three

SURFACE and INTERFACE ANALYSIS

independent injections (20 μl of injection volume) at mobile phase flow rate of 1.0 ml min^{-1}.

A standard curve of peak height against concentration of AS25 (in μg per μl) was plotted. The unknown amount of AS25 in the mixture of octanol–water solution can be obtained from the plotted standard curve. The octanol–water model system will allow us to predict the amount of water soluble antibody interacting with the biological membrane. Octanol best represents the biological membrane; hence, octanol–water partition coefficient, K_{ow}, provides useful information of the distribution of substance into two immiscible phases.[39–43]

The octanol–water partition coefficient, K_{ow}, is defined as[40,41]

$$K_{ow} = \frac{[AS25\ \ in\ \ \text{octanol-water}]}{[AS25\ \ in\ \ water]} \quad (8)$$

where the concentration of AS25 in water and octanol–water are expressed in μM, respectively.

Y-type deposition of pure C18 fatty acids and binary mixtures of C18 fatty acid/AS25 on solid substrate

Silicon (100) wafers (Sigma Aldrich, USA) were cut into pieces (5 cm × 1 cm) and placed in furnace (Carbolite, USA) for 8 h at 900 °C to allow oxidation. The oxidized silicon wafer was clamped vertical to the subphase and immersed into the dipping well before spreading the monolayer materials. Spreading solutions of C18 fatty acids were prepared in analytical-grade chloroform (Merck), respectively. After spreading, the monolayers of fatty acid were left to equilibrate for about 5 min, and 50 μl of antibody was then added onto each monolayer formed using a Hamilton microsyringe precise to 0.5 μl. The monolayer was compressed at 10 mm min^{-1} by using the same Langmuir system as above.

The Y-type deposition of LB bilayer film was performed at targeted pressure with dipping speed of 10 mm min^{-1}. The bilayer of Y-type LB film is formed when the monolayer deposits onto the oxidized silicon substrate in up and down dipping direction, which will give the head–tail–tail–head structure. A targeted surface pressure was carefully decided by referring to surface pressure (π)–molecular area (A) isotherms and compressibility analysis of pure C18 fatty acids (Fig. 1), AS25 (Fig. 2), and mixtures of C18 fatty acid/AS25 (Fig. 3). Deposition of pure SA floating monolayer on solid substrate was carried out at surface pressure of 45 mN m^{-1} and mixed system of SA/AS25 at 25 mN m^{-1}; and at 20 mN m^{-1} for the unsaturated C18 fatty acids (L1, L2, L3) and their mixed systems. AS25 floating monolayer was performed at 30 mN m^{-1}. All the transferred LB films were kept for a week in a dry, clean, and closed container before AFM imaging.

TM-AFM imaging

High-resolution imaging of bilayers was performed by TM-AFM after the floating monolayers transferred onto the oxidized silicon solid substrate from air/water interface. LB films on solid substrates

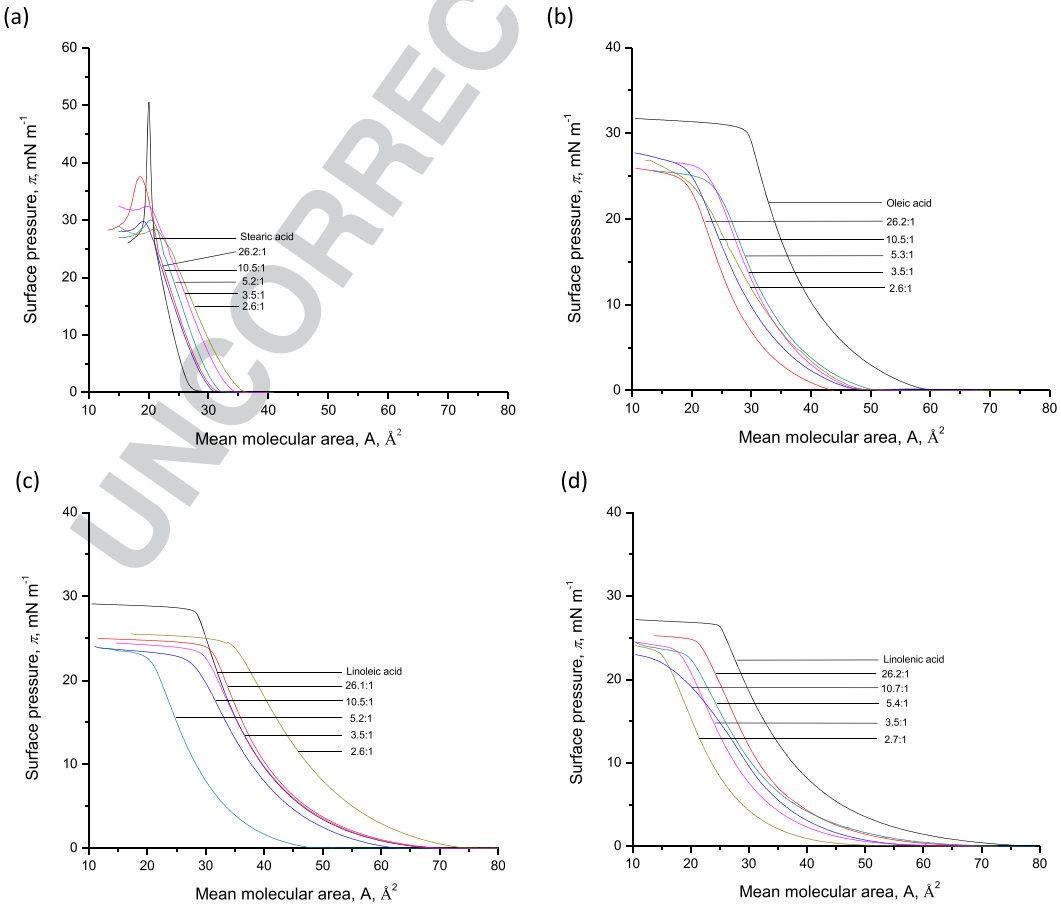

Figure 1. The surface pressure–area (π–A) isotherms of mixed monolayers (plotted in mole ratio of C18 fatty acids to anti-SNAP25): (a) stearic acid/anti-SNAP25, (b) oleic acid/anti-SNAP25, (c) linoleic acid/anti-SNAP25, and (d) linolenic acid/anti-SNAP25, spread on water subphase at 26 °C.

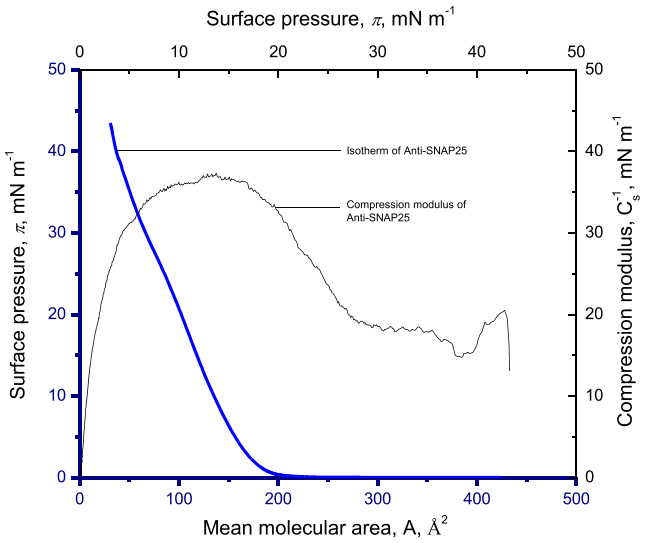

Figure 2. The surface pressure–area (π–A) isotherm of anti-SNAP25 monolayer and, its compressibility modulus (C_s^{-1}), spread on water subphase at 26 °C.

were imaged using NanoScope®V scanning probe microscope controller (Bruker, USA) in TM under ambient conditions. Silicon probes with aluminum coating (VISTA T190R, nanoScience Instrument, Canada) were used. Resonance frequency of the probe was 190 kHz, and the force constant was 48 N m^{-1}. Images in height mode were collected simultaneously with 512 × 512 points at a scanning rate of 1.0 Hz per line. All images were processed using NanoScope Analysis 1.5.

Results and discussion

Isotherms

Shown in Fig. 1 are the π–A isotherms of fatty-acid monolayers and mixed monolayers of C18 fatty acids (SA, L1, L2, and L3) with increasing volume of AS25 on nanopure water. The limiting molecular areas of pure SA, L1, L2, and L3 monolayers were determined by extrapolating the linear slope of individual π–A isotherms to zero surface pressure and were found to be 21 Å^2, 43 Å^2, 42 Å^2, and 42 Å^2, respectively. The collapse pressure of SA was found to be 50 ± 2 mN m^{-1}, which is similar to the mostly reported collapse pressure of SA at 25 °C,[44–46] some obtained at 55 mN m^{-1} but at a lower temperature, which was 20°C.[24,47] In one of Iribarnegaray *et al.* (2000) publications, it was shown that the monolayers have lower collapse pressure as the temperature of water subphase increases.[48]

When AS25 was incorporated into the SA monolayer, the isotherms of the mixed monolayers were shifted to higher surface pressures with increasing volume of AS25 (Fig. 1a). There is no specific trend on the shift shown in mixed monolayers of unsaturated fatty-acid (L1, L2, and L3) isotherms (Fig. 1b–d) with the addition

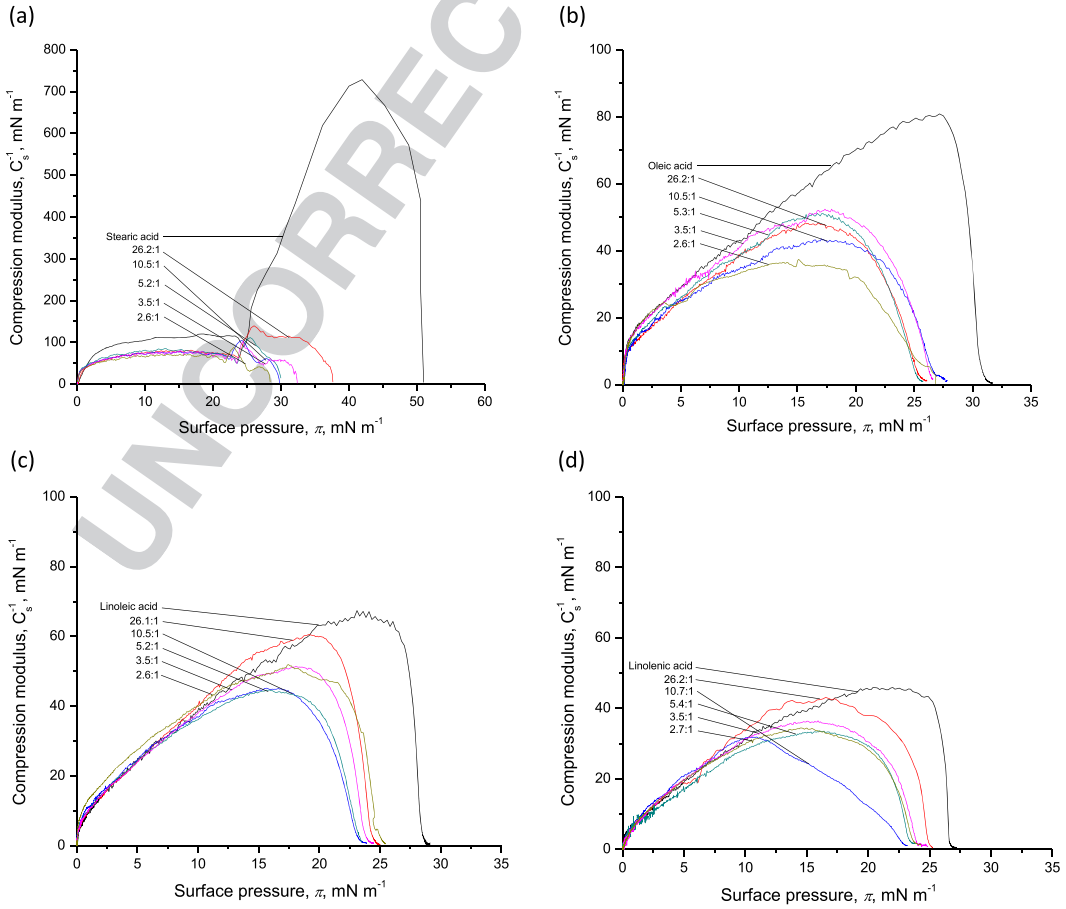

Figure 3. The compressibility modulus (C_s^{-1}) *versus* surface pressure (π) of mixed monolayers (plotted in mole ratio of C18 fatty acids to anti-SNAP25): (a) stearic acid/anti-SNAP25, (b) oleic acid/anti-SNAP25, (c) linoleic acid/anti-SNAP25, and (d) linolenic acid/anti-SNAP25, spread on water subphase at 26 °C.

SURFACE and INTERFACE ANALYSIS

of AS25; however, isotherms of the mixed systems are significantly shifting away from their pure fatty-acid isotherms in the presence of an antibody. This shows that interactions have taken place between the fatty acids and the antibody.

There was no collapse pressure clearly observed in AS25 isotherm (Fig. 2). However, the derivative of the pure-AS25 C_s^{-1} *versus* π profile (Fig. 2) showed a change at 38 mN m^{-1} that presumably corresponds to its collapse pressure. The limiting area of AS25 was found to be 160 Å^2 (Fig. 2), showing that AS25 are much larger than C18 fatty acids. There is a change in the slope that can be observed at 28 to 30 mN m^{-1}. This change is more obviously seen in its plot of C_s^{-1} *versus* π (Fig. 2), indicating that the monolayer of AS25 is low compressible and less ordered, where low C_s^{-1} values suggests that the organization of molecules of AS25 favors their arrangement in liquid-expanded (LE) phase in water subphase at 26 °C. The isotherm of AS25 is used as a reference for us to compare lipid–protein interactions and protein–protein interactions that take place in our studies.

Compressibility analysis

The packing density of monolayers can be evaluated and analyzed by the compression modulus C_s^{-1},[49,50] which is defined as

$$C_s^{-1} = -A\left(\frac{d\pi}{dA}\right). \quad (1)$$

C_s^{-1} versus π c
urves provide detailed information on phase transitions of C18 fatty-acid/AS25 monolayers (Fig. 3a–d). C_s^{-1} can be classified into various phases, namely (i) LE phase at surface pressure from 10 to 50 mN m^{-1}; (ii) liquid (L) phase from 50 to 100 mN m^{-1}; (iii) liquid-condensed (LC) phase from 100 to 250 mN m^{-1}; and (iv) solid (S) phase above 250 mN m^{-1}. In this work, the compression moduli were obtained by numerical calculation of the first derivative from the isotherm data point using the OriginPro-8 program.

Pure SA monolayers are highly condensed as supported by the large value of compression modulus in Fig. 3a. A noticeable phase transition of pure SA occurs from liquid phase (at 20 to 25 mN m^{-1}) to solid phase (at 25 to 50 mN m^{-1}); however, as for its mixed systems, there is not much change in the phase transition that can be observed in the C_s^{-1} *versus* π plot (Fig. 3a), where they remain at liquid phase 50 to 100 mN m^{-1} for the entire compression.

There is an obvious difference observed in the compressibility plot of pure SA monolayers and its mixed monolayers in the presence of antibodies at lower surface pressure (Fig. 3a). At higher surface pressure, there are some interesting observations obtained by comparing the compression-modulus profiles of SA/AS25 and pure AS25. We can observe a similar pattern in both curves at surface pressures of 28 to 32 mN m^{-1}. AS25 is known a membrane-bound protein; this behavior is clearly shown in the analysis of the binary mixed monolayer of SA/AS25. SA can be easily compressed to form a monolayer at solid phase because of the saturated hydrocarbon chain.

Molecular rearrangement of AS25 takes place in the mixtures during compression of barriers in order to accommodate the behavior of SA molecules, rod-like molecules with all *trans*-conformation in its saturated hydrocarbon chain. Once the monolayer of SA is formed and the molecules are tightly packed uniformly, AS25 interacts with SA headgroup peripherally and does not interact with SA as an integral protein, interacting spontaneously with phospholipids in natural biological membranes, as reported in our previous study.[51]

Intermolecular interactions between amphipilic fatty acids and AS25 molecules can be studied in depth by interpreting protein sequences in SNAP-25 in order to obtain better insight. SNAP-25 protein sequences are made of 206 amino acids,[30] including 63 hydrophobic, 69 hydrophilic, 44 acidic, and 30 basic amino acids. Polarity of SNAP-25 can be predicted by studying the side chain of each amino acid in the sequences, where hydrophilic amino acids will attract to the polar headgroup region of fatty acids, and hydrophobic amino acids will attract to the non-polar hydrocarbon chain. However, this prediction is insufficient to explain the behavior of AS25 in the membrane; their interactions are also affected by membrane fluidity which is related to the degree of saturation of the hydrocarbon chain, and also the headgroup of the lipids.

In this work, the investigated C18 fatty acids possess the same headgroup, but different saturation degrees in their hydrocarbon chain. The presence of *cis*-bonds in hydrophobic chains affects its geometry structure: the more *cis*-double bonds, the more bent is the chain. The presence of double bonds prevents them from packing tightly together, which allows more favorable packing of the molecules in the mixed monolayer. The maximum compression modulus values of pure-L1 and -L2 monolayers are approximately 80 mN m^{-1} and 65 mN m^{-1} respectively, and the pure-L3 monolayer, which is an unsaturated fatty acid with three double bonds, has the lowest compression modulus value, 45 mN m^{-1} (Fig. 3b–d). Unsaturated fatty acids are less compressible compared to saturated fatty acids because of their *cis*-double bonds in the hydrocarbon long chain. No phase transition is observed in these three unsaturated fatty acids. They are either at LE or L phase. Theoretically, LE and L phases in monolayers are ideal for antibodies to be embedded in between the fatty acids. Mixed systems of L1 and L2 have lower compression moduli compared to their pure systems, which are below 50 mN m^{-1}. The phase of the monolayers changes from L to LE phase. The L3 mixed system has a similar compression-modulus value as the pure system. The AS25 compression modulus, discussed above, was also found to be LE phase. Spontaneity between antibodies on the monolayer will be discussed in depth by looking at the thermodynamic stability analysis in the following section.

Miscibility of mixed monolayer

The miscibility of the mixed monolayer components can be determined by calculating the mean molecular area A_{12}.[49,50]

For ideal mixing, A_{12} is defined as

$$A_{12} = A_1X_1 + A_2X_2 \quad (2)$$

where A_1 and A_2 are the mean molecular areas of single components at the same surface pressure and X_1 and X_2 are the mole fractions of components 1 and 2 in the mixed film. These deviations can be described quantitatively with the excess mean molecular area (A_{ex}) values.

$$A_{ex} = A_{12} - (A_1X_1 + A_2X_2) \quad (3)$$

Non-linear plots of A_{ex} show the existence of interactions between the monolayers components (Fig. 4). The strength of these interactions will also be verified based on ΔG_{mix} (Fig. 5). F4 F5

Negative deviations from ideality are observed in all the mixed systems (Fig. 4). These deviations indicate that the monolayer components are miscible and reveal non-ideal behavior. The mixtures

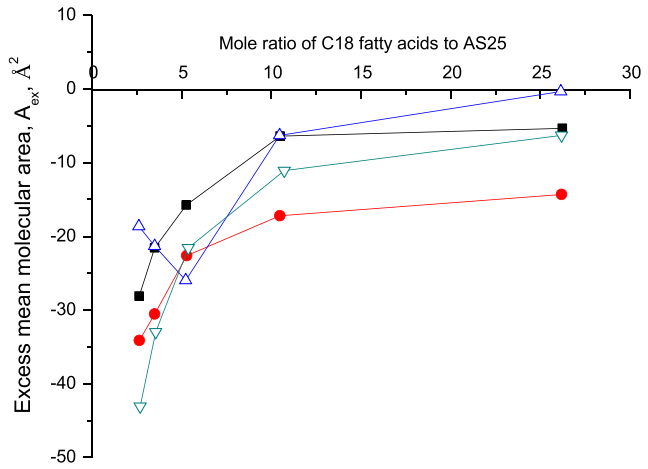

Figure 4. Excess mean molecular area (*Aex*) *versus* mole ratio of C18 fatty acids to anti-SNAP25 of mixed monolayers: ■ = stearic acid/anti-SNAP25, ● = oleic acid/anti-SNAP25, = linoleic acid/anti-SNAP25, and ▽ = linolenic acid/anti-SNAP25, spread on water subphase at 26 °C.

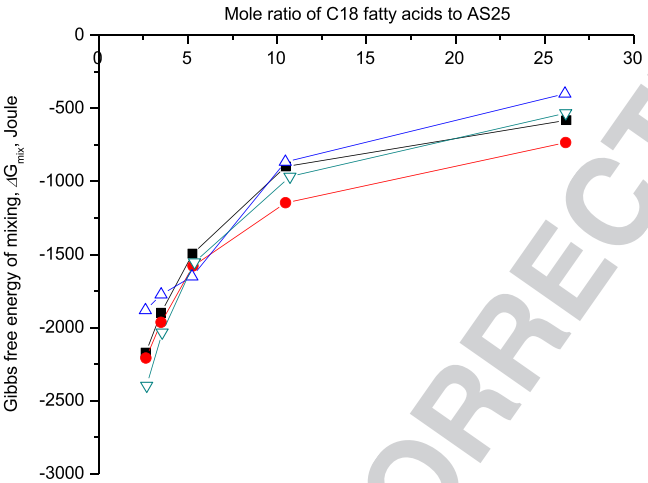

Figure 5. Gibbs free energy of mixing (*Gmix*) *versus* mole ratio of C18 fatty acids to anti-SNAP25 for mixed systems: ■ = stearic acid/anti-SNAP25, ● = oleic acid/anti-SNAP25, = linoleic acid/anti-SNAP25, and ▽ = linolenic acid/anti-SNAP25, spread on water subphase at 26 °C.

are increasingly miscible as the amount of AS25 added increased. Antibody–antibody interactions are preferable over the lipid–antibody interactions in the lipid–protein mixed systems. With the increasing mole of C18 fatty acids in mixtures, a greater repulsion between the molecules is observed in the mixed system, showing that AS25 interacts weakly with C18 fatty-acid molecules. The similar trend of intermolecular interactions occurred is also supported by the observed ΔG_{mix}, which will be discussed further in the section concerning the thermodynamic stability of the mixed monolayer.

Thermodynamic stability

Molecular interactions can be expressed quantitatively in thermodynamic analysis. The total Gibbs free energy of mixing, ΔG_{mix} is defined by the following equation,[49,50]

$$\Delta DG_{mix} = \Delta DG_{id} + \Delta DG_{ex} \quad (4)$$

where

$$\Delta DG_{id} = RT\,(X_1 lnX_1 + X_2 lnX_2). \quad (5)$$

And the excess Gibbs free energy of mixing, ΔG_{ex}, can be calculated from π–A isotherms by

$$\Delta Gex = \int_0^{\pi}[A12 - (X1A1 + X2A2)]d\pi \quad (6)$$

where A_{12}, A_1, and A_2 represent the area of the mixed system and the areas of components 1 and 2, respectively, and π is the surface pressure of the monolayer. If the monolayer is ideally mixed, ΔG_{ex} should be zero.

The presence of AS25 in the monolayer appears to be consistent in all four investigated C18 fatty acids mixed systems (Fig. 5). The negative values of ΔG_{mix} of SA/AS25, L1/AS25, L2/AS25, and L3/AS25 confirm the spontaneity interaction of AS25 molecules on the C18 fatty acids monolayers. The amount of AS25 incorporated into the monolayer strongly affected the thermodynamic properties of the lipid monolayers. With the increasing amount of AS25 in the lipid systems, the more negative ΔG_{mix} values were obtained. The most negative ΔG_{mix} was found when the mixed monolayer comprises the highest amount of AS25 (mixed systems of C18 fatty acids/AS25 at 2.6:1); however, less negative ΔG_{mix} values were observed when the mixtures containing higher mole of lipid (such as 26:1). In general, three possible interactions will take place in a lipid–protein mixture: lipid–lipid, lipid–protein, and protein–protein interactions. Presumably, antibody–antibody interactions are preferable over lipid–antibody interactions in the mixtures containing higher mole of antibody. A greater repulsion occurs between lipids and antibodies in the mixture of higher mole of lipid. Aggregation of proteins is energetically favorable when the concentrations of protein are high. Increasing lipid compositions of the membrane may change the system from protein-aggregation to a protein-distributed state.[52–54]

From the obtained ΔG_{mix}, we observed that the degree of unsaturation on the hydrocarbon chain did not significantly influence the intermolecular interaction between AS25 molecules on the lipid monolayer. As we mentioned earlier, AS25 is a membrane-bound protein, and a membrane-bound protein is prone to be on the membrane surface interacting with the headgroup of fatty acids, unlike integral protein that interact directly with the hydrocarbon chain.

In comparison to all the four C18 fatty acids that we studied, the strongest intermolecular interaction is observed in L1 at the investigated ranges. This is supported by the negative ΔG_{mix} value obtained. We suggest that L1 is the most suitable C18 fatty acid to be used as a targeted drug-delivery carrier, where a minimal amount of antibody is required for the strongest attraction between fatty acids and antibody to take place. This finding certainly has economic significance for researches because antibodies are very costly.

The negative ΔG_{mix} values obtained are very small negative values (approximately −0.05 to −0.25 kJ). Molecules of AS25 bound strongly on the surface of C18 fatty acid monolayer. These values are as expected as the role of antibodies in target delivery is as a facilitator to deliver the encapsulated drugs only to the targeted site without harming the human body[53–58]. Antibodies should interact with membranes and bind firmly to their surface like a peripheral protein in lipid–protein interactions.

In addition to support our findings, we found that only 20% of AS25 interacted with the hydrophobic fatty acids monolayer by

SURFACE and INTERFACE ANALYSIS

determining octanol–water partition coefficient (K_{ow}) using RP-HPLC. As illustrated in Fig. 6, the possibility of this amount AS25 interacting with the fatty acid monolayer (i) like an integral protein, or (ii) AS25 is partially embedded into the monolayer. And the remaining 80% are (iii) presence on the monolayer surface, interacting with the headgroup of fatty acids, or (iv) excess antibody remaining in the water subphase. From our quantitative energetic studies as above, the most potential intermolecular interactions that take place in the mixed monolayer systems are (2) and (3). It also important to note that K_{ow} corresponds only to the hydrophobic properties of AS25 on the membrane.[59]

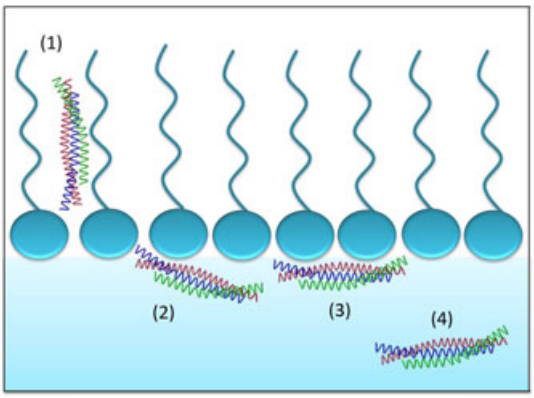

Figure 6. The possibilities of AS25 molecules interacting with the fatty acid monolayer: (1) like an integral protein, (2) AS25 is partially embedded into the monolayer, (3) presence on the monolayer surface, interacting with the headgroup of fatty acids, or (4) excess antibody remaining in the water subphase.

AFM observations

AFM topography provides a surface morphological insight into the surface interaction of pure AS25 (Fig. 7) and pure C18 fatty acids (Fig. 8), and the mixed systems of C18 fatty acids/AS25 (Fig. 9). AFM height images give useful information on film structure such as surface roughness. The mean roughness, R_a, and root mean square (rms) roughness, R_q, are the most commonly used parameter to characterize the surface features of cell membrane. Both representations of R_a and R_q demonstrate valuable information of the surface morphology and surface interactions, but they are calculated using different formulas.

R_a is the mean value of the surface relative to the center plane, calculated as[60]:

$$R_a = \frac{1}{L}\int_0^L |Z(x)|dx. \quad (7)$$

R_q is the rms of surface measurements of peaks and valleys, defined as[60]:

$$R_q = \sqrt{\frac{1}{L}\int_0^L |Z^2(x)|dx} \quad (8)$$

where $Z(x)$ is the function that describes the surface profile analyzed in terms of height (Z) and position (x) of the sample over the evaluation length of L. R_q is of a surface is similar to the

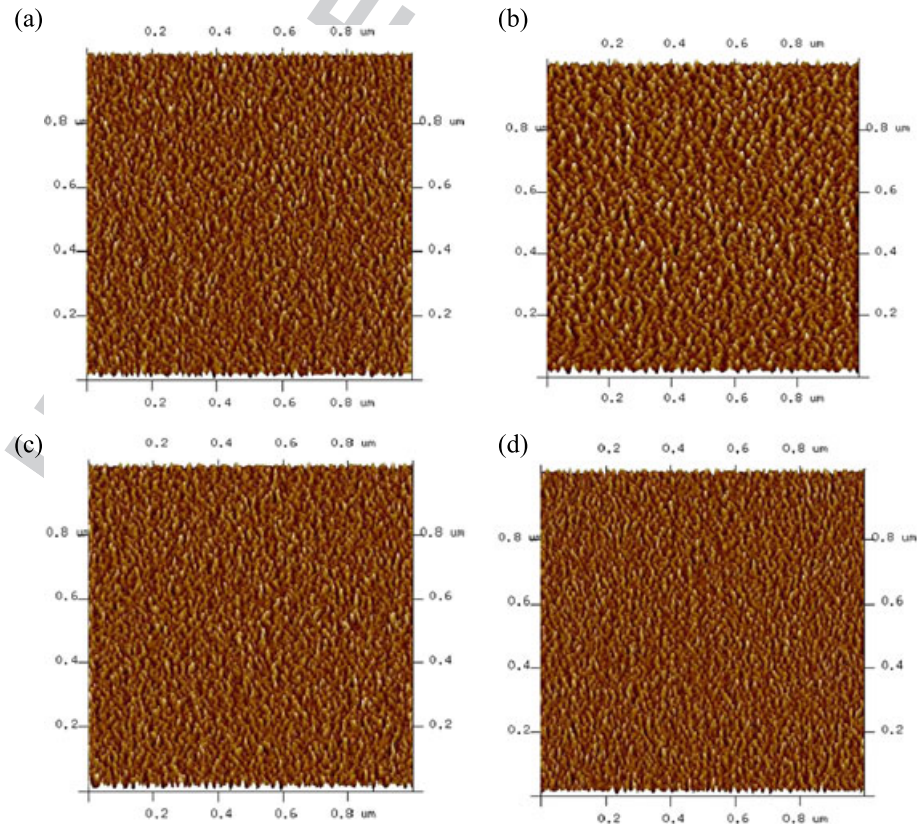

Figure 7. AFM images of pure C18 fatty-acids bilayer deposited on oxidized silicon wafer at scan size of 1 μm × 1 μm with a data scale of 25 nm for: (a) stearic acid, (b) oleic acid, (c) linoleic acid, and (d) linolenic acid.

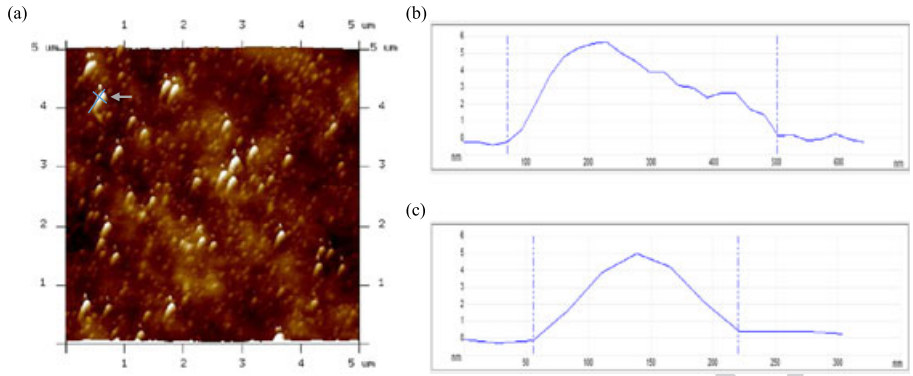

Figure 8. AFM images of pure anti-SNAP25 bilayer deposited on oxidized silicon wafer obtained in scan size of (a) 5 μm × 5 μm with a data scale of 25 nm. A cross section was drawn on a selected AS25 molecule incorporated on the membrane depicted in (a) to obtain more information of the height and width of AS25 molecule. The height (b) and width (c) of this membrane bound protein were found to be 453 nm × 166 nm, respectively. Protein structure predictions of AS25 from its protein sequences that it is a coiled-coil structure as illustrated in Fig. 6[29] and our scanned images as above showed the shape of AS25 is true as predicted.

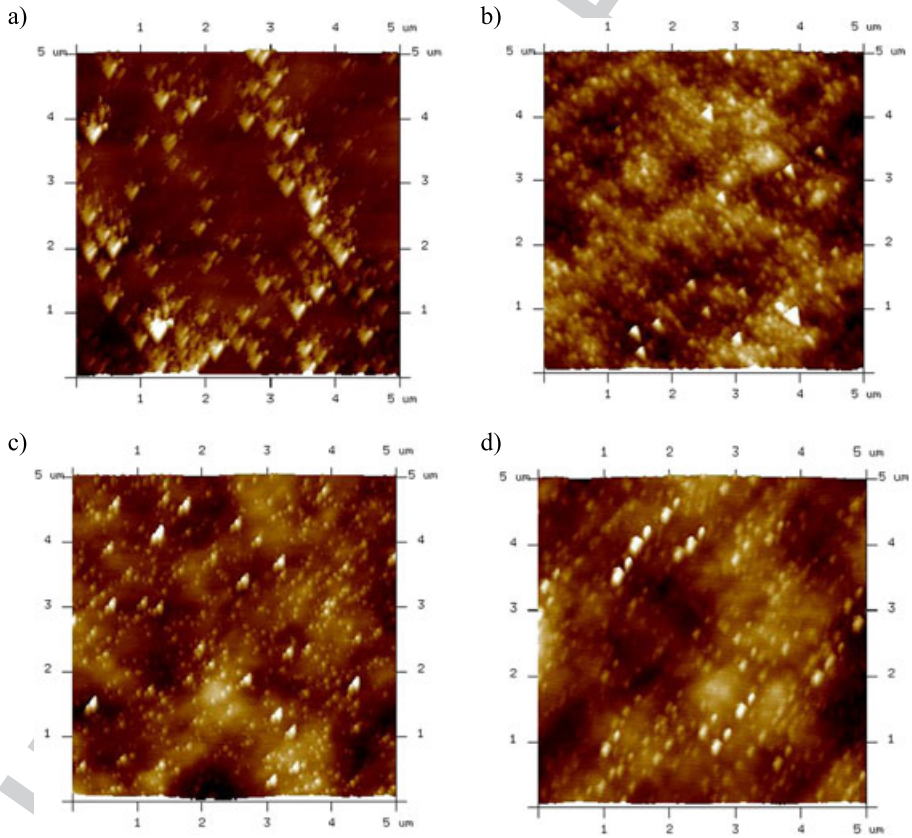

Figure 9. AFM images of binary mixture of C18 fatty acids/AS25 bilayer deposited on oxidized silicon wafer obtained in a 5.0 μm × 5.0 μm scan area with a data scale of 25 nm for: (a) stearic acid/AS25, (b) oleic acid/AS25, (c) linoleic acid/AS25, and (d) linolenic acid/AS25.

roughness average, R_a, with the only difference being the mean squared absolute values of surface roughness profile.

The obtained R_a and R_q values for all surfaces of pure AS25, C18 fatty acids, and mixed systems in this manuscript were obtained by using NanoScope Analysis 1.5 (Table 1). The differences of between the surface roughness give us some idea of the changes of surface texture of pure and mixed systems.

R_a and R_q values of pure C18 fatty acids increase with the increasing degree of saturation of C18 fatty acids. In contrast, for the mixed systems of C18 fatty acid/AS25, we observed both parameters R_a and R_q decrease with the increasing double bonds in their hydrocarbon chains. The degree of saturations induces greater penetration of AS25 on the lipid bilayers. In the pure system of SA (a saturated fatty acid) and mixed system of SA/AS25, R_a values increases dramatically from 0.215 to 0.721 nm. On the contrary, only a slight increase of R_a is observed for L3 (unsaturated fatty acid) and L3/AS225, which is from 0.460 to 0.493 nm.

The surface of pure C18 fatty acids is relatively flat; hence, R_q increases by about 0.1 to the respective R_a values. More peaks and valleys are observed in the mixed systems of C18 fatty

SURFACE and INTERFACE ANALYSIS

Table 1. Surface roughness, R_a and R_q of pure C18 fatty acids, AS25, and mixed systems of C18 fatty acids/AS25 bilayer membrane (obtained using NanoScope Analysis 1.5)

Pure systems	Surface roughness, nm		Mixed systems	Surface roughness, nm	
	R_a	R_q		R_a	R_q
SA	0.215	0.286	SA/AS25	0.721	1.010
L1	0.249	0.303	L1/AS25	0.543	0.701
L2	0.428	0.578	L2/AS25	0.528	0.584
L3	0.460	0.575	L3/AS25	0.493	0.630
AS25	0.566	0.789			

acids/AS25, R_q is found to be much larger than R_a, as R_q values will be significantly affected (more than R_a) when the surface contains a large number of peaks and valleys in the mixtures, owing to the squaring of the amplitude in the calculation. The values of R_a and R_q of mixed systems of C18 fatty acids/AS25 are greatly affected by the degree of saturation of C18 fatty acids. We observed that the R_q value of saturated SA/AS25 is different by 0.28 (as R_a is 0721 and R_q is 1.010), while unsaturated L1/AS25, L2/AS25, and L3/AS25 are only different by about 0.15. This could be more peaks and valleys appear on the surface of SA/AS25 as more AS25 molecules were bounded on the saturated SA membrane surface. R_q of SA/AS25 is found to be larger than of AS25; this shows that more AS25 molecules are bounded on the surface as a result from the tightly packed of saturated SA bilayer. From our energetic studies, ΔG_{mix} of all mixed systems is not remarkably affected by degree of saturation of C18 fatty acids' hydrocarbon chain. However, our AFM surface roughness analysis supports our hypothesis on how the membrane-bound AS25 antibody interacts with C18 fatty acids with different degree of saturation. In the mixed systems of unsaturated L1/AS25, L2/AS25, and L3/AS25, the *cis*-double bond(s) prevent the tight and rigid molecular packing enable AS25 molecules partially embedded into the bilayer membrane as illustrated in Fig. 6. Thus, less peaks and valleys are observed as we compare them to SA/AS25 mixed system. We conclude that AS25 molecules are bounded on saturated SA's carboxyl headgroup, but partially inserted into unsaturated C18 fatty acid membrane.

AFM observations from this study supported our quantitative analysis which indicated that AS25 molecules are bounded on the membrane surface as predicted theoretically.

Conclusion

AS25, a membrane-bound protein, has become our choice of protein to explore lipid–protein interactions. In this study, we have shown how a peripheral protein interacts with fatty acids with the support of thermodynamic quantitative data, as fatty acids are essential structural elements of biological membranes. Langmuir monolayers of lipid–protein mixed systems were successfully used to illustrate the lipid–protein interactions occurring in natural biological membranes. Lipid–protein interactions are crucial in developing targeted liposomal DDS formulations. The composition ratio of lipids and antibodies in forming DDS can be determined precisely from the energetic stability of the mixed system, which will also allow us to ensure that antibodies are successfully incorporated to the lipid-carrier system. The energetic investigation of AS25-C18 fatty-acid mixtures enabled us to draw the conclusion that AS25 molecules bound strongly on the C18 fatty acids monolayer, with the support of RP-HPLC and AFM surface roughness analysis. L1 can be considered the best C18 fatty acid that interacted with AS25 in a binary system. A very small amount of AS25 incorporated into the L1 membrane model caused the strongest interactions to take place, where the mole ratio of L1/AS25 was 26 to 1. This L1/AS25 ratio mimicking a half bilayer membrane is very useful reference for our future studies in preparing fatty acid nanoliposomes as targeted drug-delivery vehicles. L1 is rather less expensive compared to the other two unsaturated lipids investigated. It is also important for us to note that not excessive amounts of antibodies should be introduced into human body. A large amount of antibodies will harm the human body, and it is not economically feasible as the cost of antibodies is extremely expensive, even at very small volumes.

Acknowledgements

This study was financially supported by the Fundamental Research Grant Scheme (FP001-2013A), UM-MoHE High Impact Research Grant (F000009-21001), and UMRG Flagship (FL001F-131310), Malaysia. Gew would like to thank Phra Phrom for all blessing.

References

[1] A. Chonn, P. R. Cullis, *Adv. Drug Deliv. Rev.* **1998**, *30*, 73–83.
[2] E. Mastrobattista, G. A. Koning, G. Storm, *Adv. Drug Deliv. Rev.* **1999**, *40*, 103–27.
[3] V. P. Torchilin, *Nat. Rev. Drug Discov.* **2005**, *4*, 145–60.
[4] H. I. Chang, M. K. Yeh, *Int. J. Nanomedicine* **2012**, *7*, 49–60.
[5] J. W. Park, D. B. Kirpotin, K. Hong, R. Shalaby, Y. Shao, U. B. Nielsen, J. D. Marks, D. Papahadjopoulos, C. C. Benz, *J. Control. Release* **2001**, *74*, 95–113.
[6] B. B. Lundberga, G. Griffithsb, H. J. Hansen, *J. Control. Release* **2004**, *94*, 155–61.
[7] K. Laginha, D. Mumbengegwi, T. Allen, *Biochim. Biophys. Acta* **2005**, *1711*, 25–32.
[8] N. Debottona, M. Parnesa, J. Kadoucheb, S. Benita, *J. Control. Release* **2005**, *127*, 219–30.
[9] A. S. Manjappa, K. R. Chaudhari, M. P. Venkatarajua, P. Dantuluri, B. Nanda, C. Sidda, K. S. Krutika, S. Rayasa, M. Ramachandra, *J. Control. Release* **2011**, *150*, 2–22.
[10] T. Mita, *Bull. Chem. Soc. Japan.* **1989**, *62*, 3114–21.
[11] A. G. Lee, *Biochim. Biophys. Acta* **2003**, *1612*, 1–40.
[12] C. Stefaniu, G. Brezesinski, H. Möhwald, *Adv. Colloid Interface Sci.* **2014**, *208*, 197–213.
[13] A. P. Girard-Egrot, S. Godoy, L. J. Blum, *Adv. Colloid Interface Sci.* **2005**, *116*, 205–25.
[14] H. G. Hansma, L. Pietrasanta, *Curr. Opin. Chem. Biol.* **1985**, *2*, 79–84.
[15] B. Basnar, G. Friedbacher, H. Brunner, T. Vallant, U. Mayer, H. Hoffmann, *Appl. Surf. Sci.* **2001**, *171*, 213–25.
[16] J. Li, R. Sun, C. Hao, G. He, L. Zhang, J. Wang, *Biophys. Chem.* **2015**, *205*, 33–40.
[17] J. L. Alonso, W. H. Goldmann, *Life Sci.* **2003**, *72*, 2553–60.
[18] N. C. Santos, M. A. Castanho, *Biophys. Chem.* **2004**, *107*, 133–49.
[19] H. Palsdottir, C. Hunte, *Biochim. Biophys. Acta* **2004**, *1666*, 2–18.
[20] C. Hunte, S. Richers, *Curr. Opin. Chem. Biol.* **2008**, *18*, 406–11.
[21] A. Laganowsky, E. Reading, T. M. Allison, M. B. Ulmschneider, M. T. Degiacomi, A. J. Baldwin, C. V. Robinson, *Nature* **2014**, *510*, 172–5.
[22] J. R. Kanicky, D. O. Shah, *J. Colloid Interface Sci.* **2002**, *256*, 201–7.
[23] D. Vollhardt, *J. Phys. Chem. C* **2007**, *111*, 6805–12.
[24] K. Hąc-Wydro, P. Wydro, *Chem. Phys. Lipids* **2007**, *150*, 66–81.
[25] K. Hąc-Wydro, K. Jędrzejek, P. Dynarowicz-Łątka, *Colloids Surf. B Biointerfaces* **2009**, *72*, 101–11.
[26] T. L. Glassa, T. D. Raabeb, D. M. Garcıaa, J. R. Kokea, *Brain Res.* **2002**, *934*, 43–8.
[27] T. Hasegawa, M. Matsuzaki, A. Takeda, A. Kikuchi, K. Furukawa, S. Shibahara, Y. Itoyama, *J. Neurochem.* **2003**, *87*, 470–475.
[28] R. Constantinescu, A. T. Constantinescu, H. Reichmann, B. Janetzky, *J. Neural Transm.* **2007**, *72*, 17–28.

[29] Y. T. Cheung, W. K. W. Lau, M. S. Yu, C. S. W. Lai, S. C. Yeung, K. F. So, R. C. Chang, *NeuroToxicology* **2009**, *30*, 127–35.
[30] A. Hodel, *Int. J. Biochem. Cell Bio* **1998**, *30*, 1069–73.
[31] J. E. Rothman, *Nature* **1994**, *372*, 55.
[32] J. Zimmerberg, S. S. Vogel, L. V. Chernomordik, *Annu. Rev. Biophys. Biomol. Struct.* **1993**, *22*, 433–66.
[33] Z. Joshua, L. V. Chernomordik, *Adv. Drug Deliv. Rev.* **1999**, *38*, 197–205.
[34] H. R. Marsden, I. Tomatsu, A. Kros, *Chem. Soc. Rev.* **2011**, *40*, 1572–85.
[35] J. E. Rothman, *Ang. Chem. Int. Ed.* **2014**, *53*, 12676–94.
[36] G. Cevc, H. Richardsen, *Adv. Drug Deliv. Rev.* **1999**, *38*, 207–32.
[37] M. Ma, D. Bong, *Acc. Chem. Res.* **2013**, *46*, 2988–97.
[38] T. Nakamura, K. W. Peng, S. Vongpunsawad, M. Harvey, H. Mizuguchi, T. Hayakawa, R. Cattaneo, S. J. Russell, *Nat. Biotechnol.* **2004**, *22*, 331–6.
[39] R. G. Efremov, A. O. Chugunov, T. V. Pyrkov, J. P. Priestle, A. S. Arseniev, E. Jacoby, *Curr. Med. Chem.* **2007**, *14*, 393–415.
[40] A. Leo, C. Hansch, D. Elkins, *Chem. Rev.* **1971**, *71*, 525–616.
[41] J. Sangster, *J. Phys. Chem. Ref. Data.* **1989**, *18*, 1111–229.
[42] A. Berthod, S. Carda-Broch, *J. Chromatogr., A* **2004**, *1037*, 3–14.
[43] J. F. Nagle, J. C. Mathai, M. L. Zeidel, S. Tristram-Nagle, *J. Gen. Physiol.* **2008**, *131*, 77–85.
[44] T. Kamilya, P. Pal, G. B. Talapatra, *Colloids Surf. B Biointerfaces* **2007**, *58*, 137–44.
[45] A. C. Teixeira, A. C. Fernandes, A. R. Garcia, L. M. Ilharco, P. Brogueira, A. M. Goncalves da Silva, *Chem. Phys. Lipids* **2007**, *149*, 1–13.
[46] S. Kundu, D. Langevin, *Colloids Surf. A.* **2008**, *325*, 81–5.
[47] P. Wydro, B. Krajewska, K. Hąc-Wydro, *Biomacromolecules* **2007**, *8*, 2611–7.
[48] R. Seoane, J. Miñones, O. Conde, J. Miñones, M. Casas, E. Iribarnegaray, *J. Phys. Chem. B* **2000**, *104*, 7735–44.
[49] J. T. Davies, E. K. Rideal, *Interfacial Phenomena*, Academic Press, New York, **1963**.
[50] G. L. Gaines, *Insoluble Monolayers at Liquid–Gas Interfaces*, Interscience, New York, **1966**.
[51] L. T. Gew, M. Misran, *Nanoscale Res. Lett.* **2014**, *9*, 218.
[52] T. Gil, J. H. Ipsen, O. G. Mouritsen, M. C. Sabra, M. M. Sperotto, M. J. Zuckermann, *Biochim. Biophys. Acta* **1998**, *1376*, 245–66.
[53] M. M. Sperotto, S. May, A. Baumgaertner, *Chem. Phys. Lipids* **2006**, *141*, 2–29.
[54] C. L. Armstrong, E. Sandqvist, M. C. Rheinstadter, *Protein Peptide Lett.* **2011**, *18*, 344–53.
[55] U. E. Nydegger, M. Sturzenegger, *Drug Saf.* **1999**, *21*, 171–85.
[56] D. J. Hamrock, *Int. Immunopharmacol.* **2006**, *6*, 535–42.
[57] T. T. Hansel, H. Kropshofer, T. Singer, J. A. Mitchell, A. J. T. George, *Nat. Rev. Drug Discov.* **2010**, *9*, 325–38.
[58] M. Harris, *Lancet Oncol.* **2004**, *5*, 292–302.
[59] M. Boroujerdi, *Pharmacokinetics and Toxicokinetics*, CRC Press, United State of America, **2015**.
[60] R. R. L. De Oliveira, D. A. C. Albuquerque, T. G. S. Cruz, F. M. Yamaji, F. L. Leite, in *Measurement of the Nanoscale Roughness by Atomic Force Microscopy: Basic Principles and Applications, Atomic Force Microscopy—Imaging, Measuring and Manipulating Surfaces at the Atomic Scale* (Ed: Dr.V. Bellitto), INTECH Open Access Publisher, Croatia, **2012**, pp. 147–175.

Author Query Form

Journal: Surface and Interface Analysis

Article: sia_6144

Dear Author,

During the copyediting of your paper, the following queries arose. Please respond to these by annotating your proofs with the necessary changes/additions.

- If you intend to annotate your proof electronically, please refer to the E-annotation guidelines.
- If you intend to annotate your proof by means of hard-copy mark-up, please use the standard proofing marks. If manually writing corrections on your proof and returning it by fax, do not write too close to the edge of the paper. Please remember that illegible mark-ups may delay publication.

Whether you opt for hard-copy or electronic annotation of your proofs, we recommend that you provide additional clarification of answers to queries by entering your answers on the query sheet, in addition to the text mark-up.

Query No.	Query	Remark
Q1	AUTHOR: Please confirm that given names (red) and surnames/family names (green) have been identified correctly.	

WILEY

USING e-ANNOTATION TOOLS FOR ELECTRONIC PROOF CORRECTION

Required software to e-Annotate PDFs: Adobe Acrobat Professional or Adobe Reader (version 7.0 or above). (Note that this document uses screenshots from Adobe Reader X)
The latest version of Acrobat Reader can be downloaded for free at: http://get.adobe.com/uk/reader/

Once you have Acrobat Reader open on your computer, click on the Comment tab at the right of the toolbar:

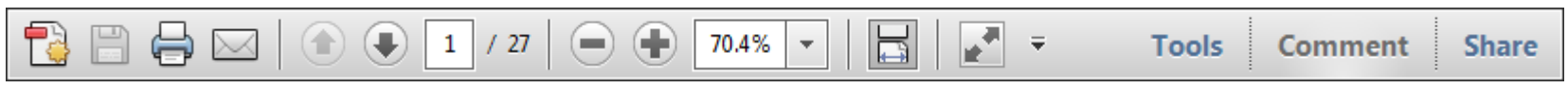

This will open up a panel down the right side of the document. The majority of tools you will use for annotating your proof will be in the Annotations section, pictured opposite. We've picked out some of these tools below:

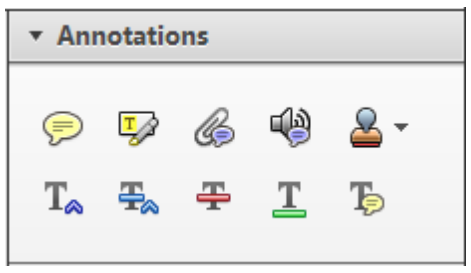

1. Replace (Ins) Tool – for replacing text.

Strikes a line through text and opens up a text box where replacement text can be entered.

How to use it

- Highlight a word or sentence.
- Click on the Replace (Ins) icon in the Annotations section.
- Type the replacement text into the blue box that appears.

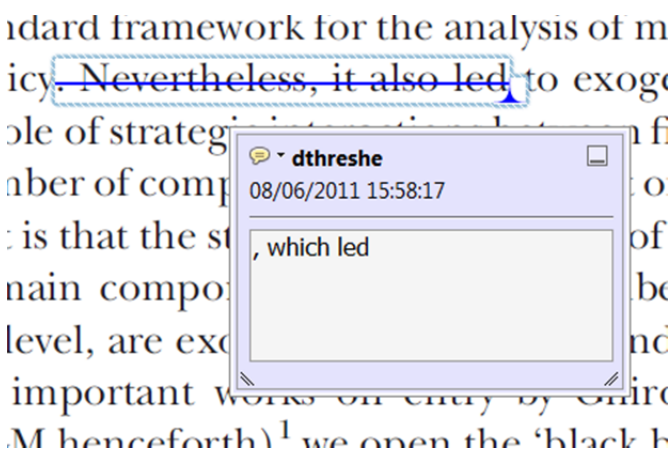

2. Strikethrough (Del) Tool – for deleting text.

Strikes a red line through text that is to be deleted.

How to use it

- Highlight a word or sentence.
- Click on the Strikethrough (Del) icon in the Annotations section.

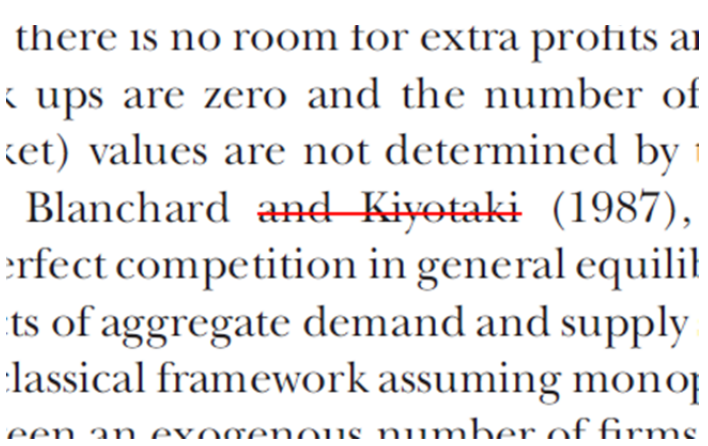

3. Add note to text Tool – for highlighting a section to be changed to bold or italic.

Highlights text in yellow and opens up a text box where comments can be entered.

How to use it

- Highlight the relevant section of text.
- Click on the Add note to text icon in the Annotations section.
- Type instruction on what should be changed regarding the text into the yellow box that appears.

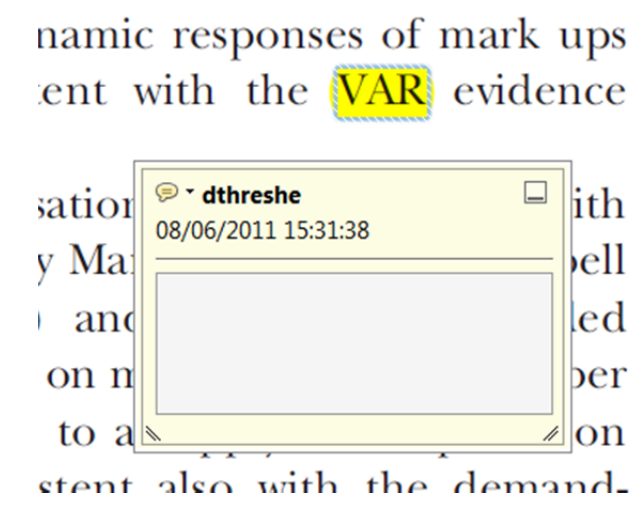

4. Add sticky note Tool – for making notes at specific points in the text.

Marks a point in the proof where a comment needs to be highlighted.

How to use it

- Click on the Add sticky note icon in the Annotations section.
- Click at the point in the proof where the comment should be inserted.
- Type the comment into the yellow box that appears.

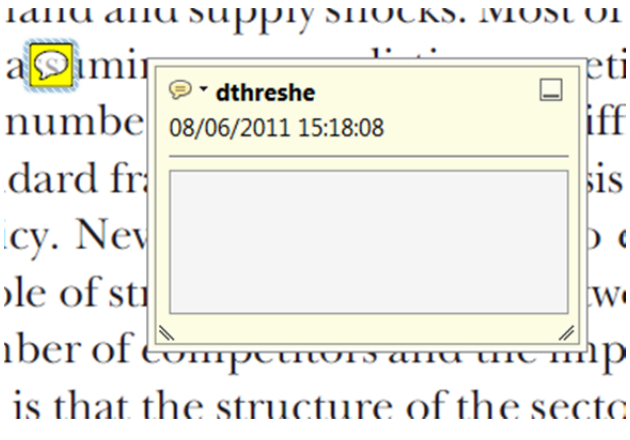

WILEY

USING e-ANNOTATION TOOLS FOR ELECTRONIC PROOF CORRECTION

5. Attach File Tool – for inserting large amounts of text or replacement figures.

Inserts an icon linking to the attached file in the appropriate pace in the text.

How to use it

- Click on the Attach File icon in the Annotations section.
- Click on the proof to where you'd like the attached file to be linked.
- Select the file to be attached from your computer or network.
- Select the colour and type of icon that will appear in the proof. Click OK.

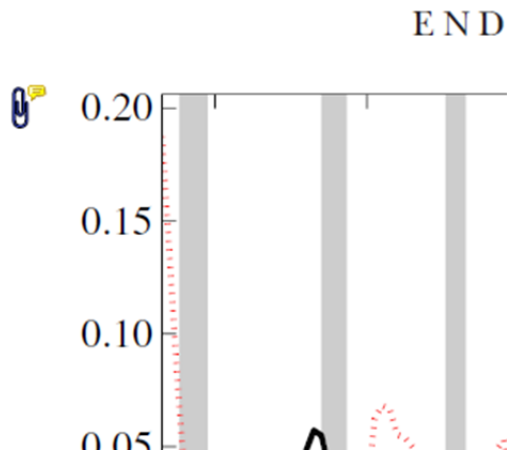

6. Add stamp Tool – for approving a proof if no corrections are required.

Inserts a selected stamp onto an appropriate place in the proof.

How to use it

- Click on the Add stamp icon in the Annotations section.
- Select the stamp you want to use. (The Approved stamp is usually available directly in the menu that appears).
- Click on the proof where you'd like the stamp to appear. (Where a proof is to be approved as it is, this would normally be on the first page).

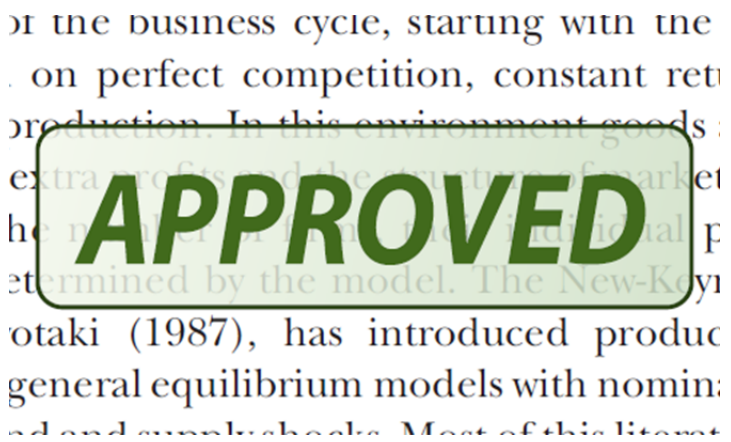

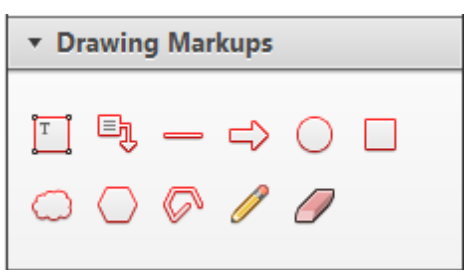

7. Drawing Markups Tools – for drawing shapes, lines and freeform annotations on proofs and commenting on these marks.

Allows shapes, lines and freeform annotations to be drawn on proofs and for comment to be made on these marks..

How to use it

- Click on one of the shapes in the Drawing Markups section.
- Click on the proof at the relevant point and draw the selected shape with the cursor.
- To add a comment to the drawn shape, move the cursor over the shape until an arrowhead appears.
- Double click on the shape and type any text in the red box that appears.

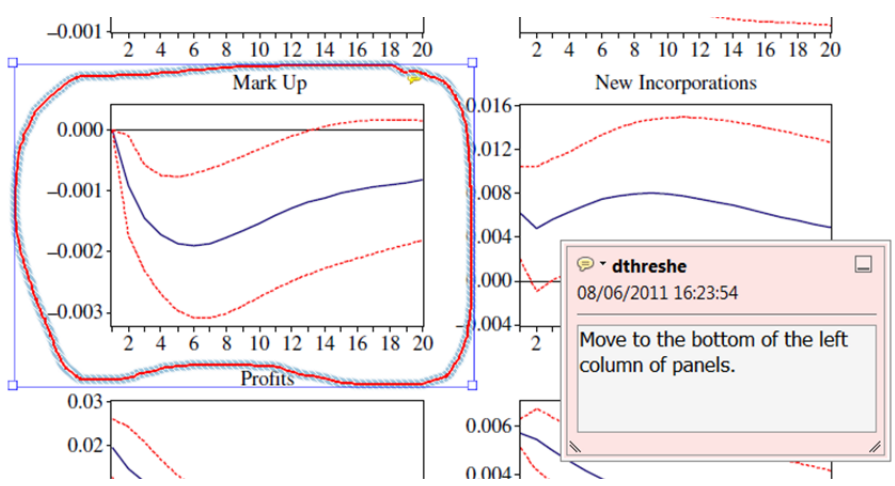

For further information on how to annotate proofs, click on the Help menu to reveal a list of further options: